Supplementary material

Table S1. Similar to Table 1, except for $(\mu_0,\ \varphi_0) = (0.1,\ 0°)$.

		$\mu = 0.1$		$\mu = 0.5$		$\mu = 1.0$	
		de Haan	MONKI	de Haan	MONKI	de Haan	MONKI
$\mu_0 = 0.5$	I	0.522770	0.522889±0.000698	0.106590	0.106610±0.000126	0.026009	0.026016±0.000028
$\varphi = 0°$	Q	0.011506	0.011517±0.000100	-0.005186	-0.005192±0.000031	-0.014984	-0.014990±0.000015
	U	0.000000	0.000017±0.000071	0.000000	0.000003±0.000027	0.000000	-0.000002±0.000009
	V	0.000000	0.000001±0.000006	0.000000	0.000000±0.000004	0.000000	0.000000±0.000001
$\mu_0 = 0.5$	I	0.276300	0.276328±0.000288	0.083628	0.083655±0.000103	0.026009	0.026016±0.000028
$\varphi = 30°$	Q	0.034368	0.034374±0.000098	0.003839	0.003844±0.000031	-0.007492	-0.007493±0.000011
	U	-0.016042	-0.016035±0.000065	-0.014492	-0.014500±0.000027	-0.012976	-0.012983±0.000014
	V	0.000027	0.000029±0.000006	0.000017	0.000017±0.000004	0.000000	0.000000±0.000001

Table S2. Similar to Table 1, except for downward emerging light at the surface (BOA).

		$\mu = 0.1$		$\mu = 0.5$		$\mu = 1.0$	
		de Haan	MONKI	de Haan	MONKI	de Haan	MONKI
$\mu_0 = 0.5$	I	1.036450	1.037420±0.003919	2.287330	2.287581±0.003720	0.088417	0.088306±0.000243
$\varphi = 0°$	Q	0.010451	0.010433±0.000450	0.007210	0.007210±0.000181	-0.023375	-0.023323±0.000099
	U	0.000000	0.000037±0.000334	0.000000	0.000014±0.000152	0.000000	-0.000002±0.000058
	V	0.000000	0.000016±0.000045	0.000000	0.000001±0.000014	0.000000	0.000001±0.000005
$\mu_0 = 0.5$	I	0.566020	0.566175±0.002438	0.604840	0.604778±0.001157	0.088417	0.088306±0.000243
$\varphi = 30°$	Q	0.013634	0.013628±0.000479	0.012593	0.012605±0.000189	-0.011687	-0.011663±0.000062
	U	-0.016244	-0.016229±0.000417	-0.002307	-0.002332±0.000148	0.020243	0.020197±0.000097
	V	0.000084	0.000093±0.000049	-0.000137	-0.000137±0.000015	0.000000	0.000001±0.000005

Table S3. Similar to Table S1, except for downward emerging light at the surface (BOA).

		$\mu = 0.1$		$\mu = 0.5$		$\mu = 1.0$	
		de Haan	MONKI	de Haan	MONKI	de Haan	MONKI
$\mu_0 = 0.5$	I	0.191930	0.191896±0.000813	0.129879	0.129907±0.000243	0.022968	0.022955±0.000049
$\varphi = 0^\circ$	Q	0.003451	0.003459±0.000122	0.000363	0.000357±0.000046	-0.013424	-0.013417±0.000035
	U	0.000000	-0.000016±0.000103	0.000000	0.000014±0.000035	0.000000	0.000005±0.000016
	V	0.000000	0.000000±0.000012	0.000000	0.000002±0.000004	0.000000	-0.000000±0.000001
$\mu_0 = 0.5$	I	0.086631	0.086356±0.000502	0.084823	0.084807±0.000222	0.022968	0.022955±0.000049
$\varphi = 30^\circ$	Q	0.006335	0.006287±0.000127	0.005860	0.005829±0.000051	-0.006712	-0.006704±0.000022
	U	0.001320	0.001336±0.000079	0.006928	0.006933±0.000041	0.011626	0.011622±0.000032
	V	-0.000010	-0.000007±0.000014	-0.000062	-0.000059±0.000004	0.000000	-0.000000±0.000001

Table S4. Viewing and solar geometries for the 9 3D cloud test cases of Emde et al. (2018), using the angular definitions of MONKI. The solar azimuth angle is $\varphi_0 = 0^\circ$ for all cases. For the cases with $\theta > 90^\circ$ the observer is at BOA, otherwise the observer is at TOA.

No.	θ_0 [°]	θ [°]	φ [°]
1	20	140	180
2	20	140	240
3	20	140	300
4	20	140	0
5	40	0	180
6	40	40	180
7	40	40	240
8	40	40	300
9	40	40	0

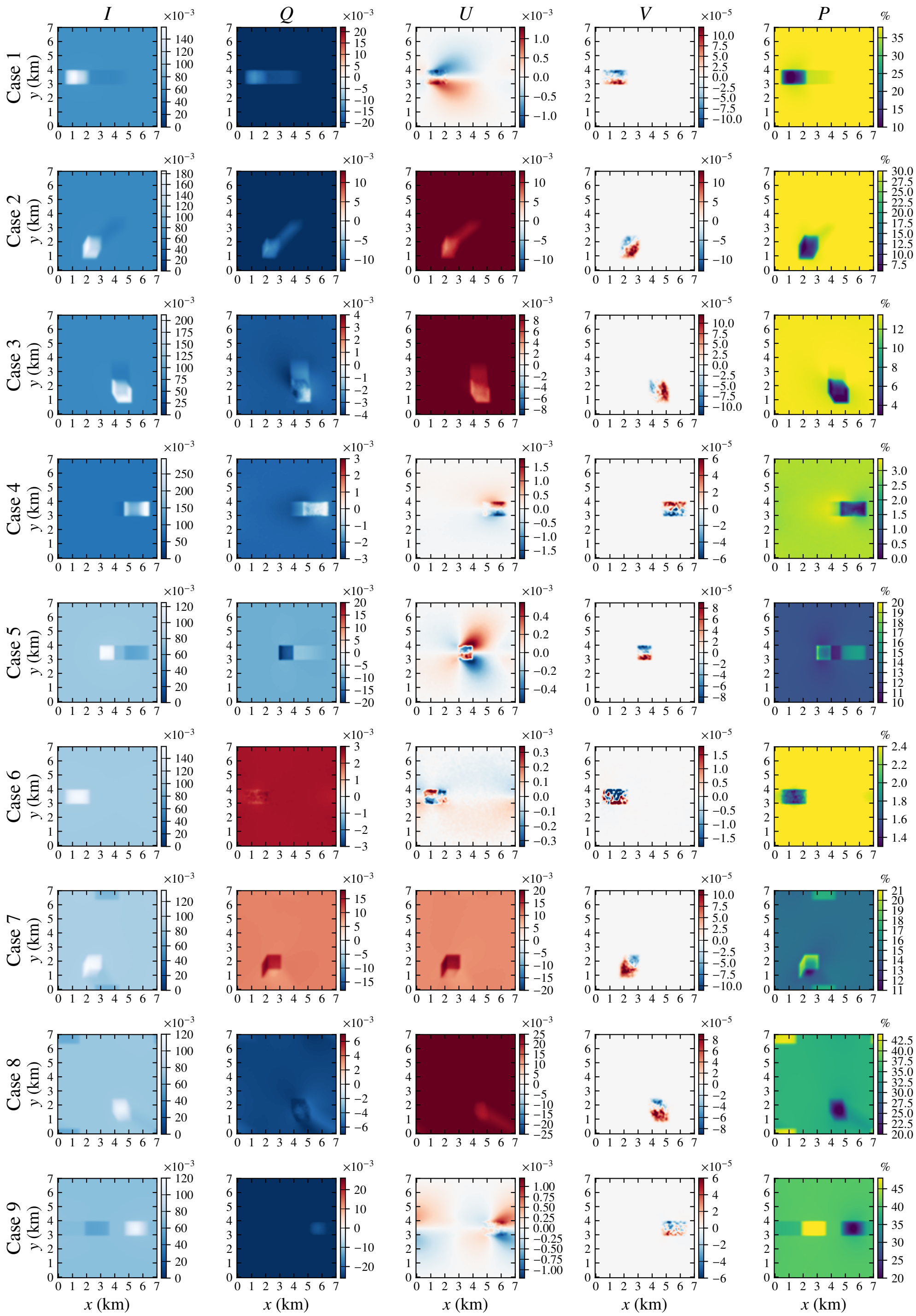

Figure S1. Similar to Fig. 5, except for all Stokes parameters I, Q, U, and V, and for degree of polarisation P (the columns), at all 9 solar and viewing geometry cases (the rows) presented in Table S4.

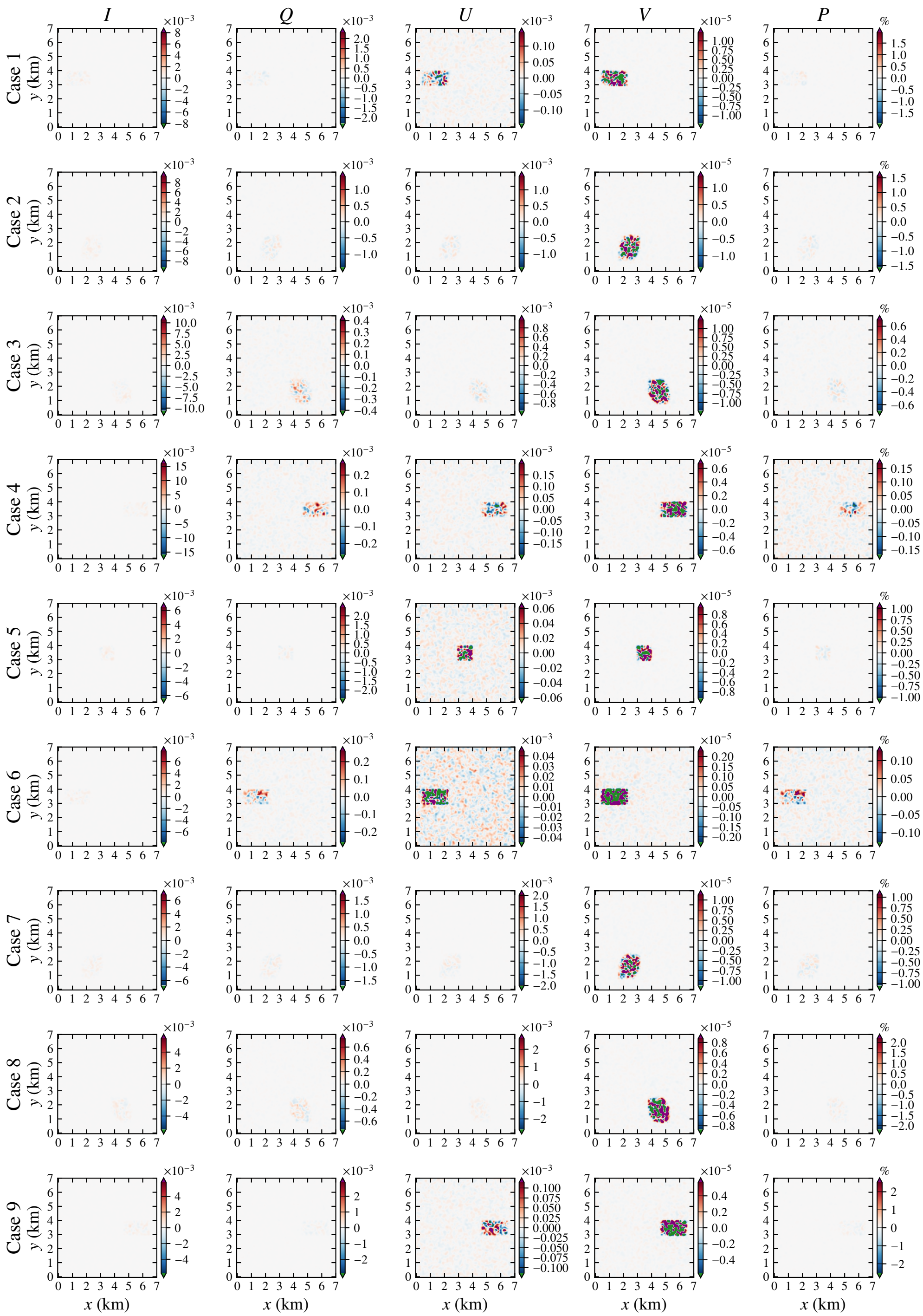

Figure S2. Similar to Fig. S1, except for the differences between MONKI and MYSTIC (see Fig. A2 of Emde et al., 2018). Following Emde et al. (2018), the limits of the colorbars are set to 5% of the maximum values for I and P, and to 10% of the values for $|Q|$ and $|U|$. Values larger than the upper limit are marked in purple and values smaller than the lower limit are marked in green.

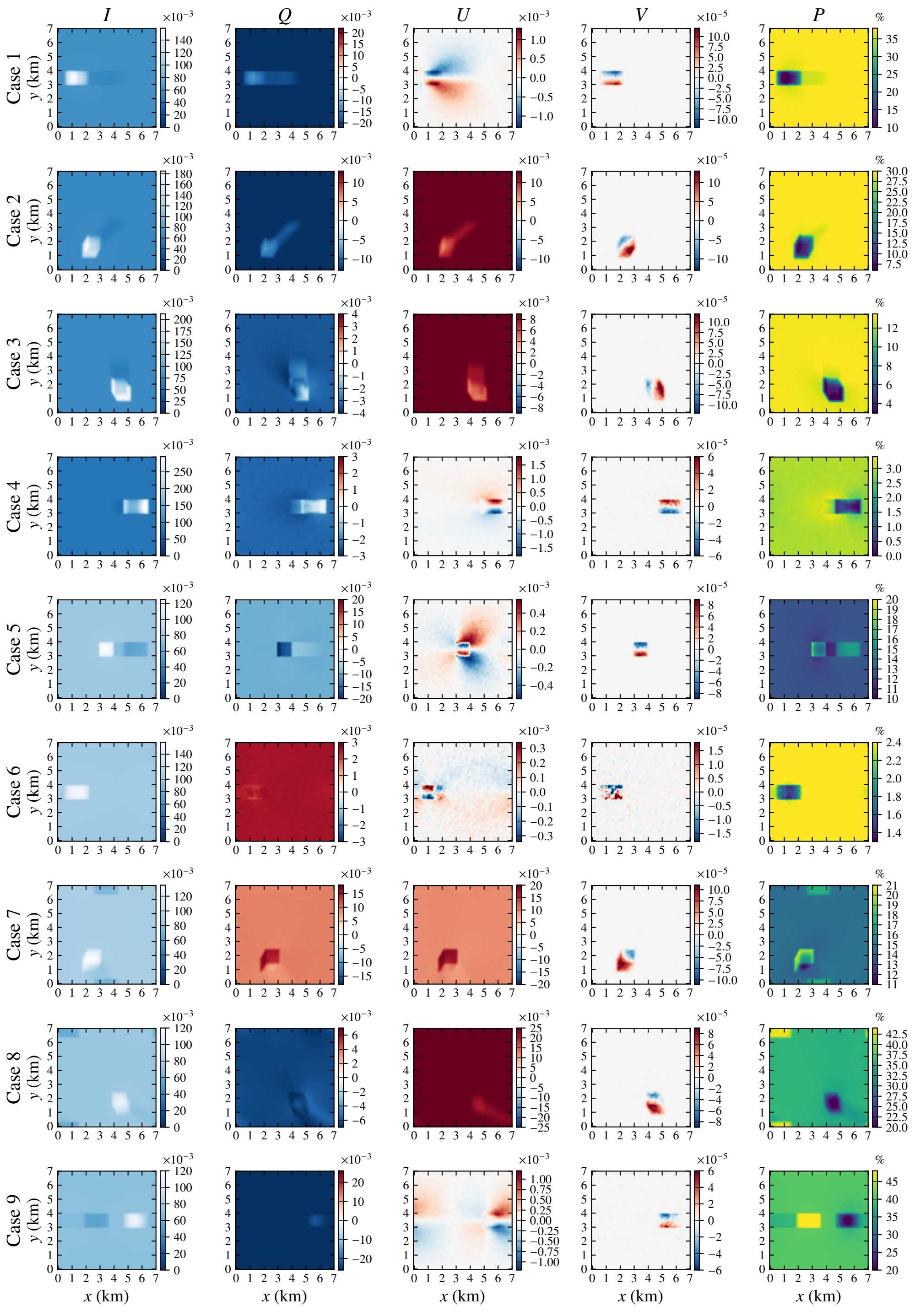

Figure S3. Similar to Fig. S1, except with MONKI in backward mode.

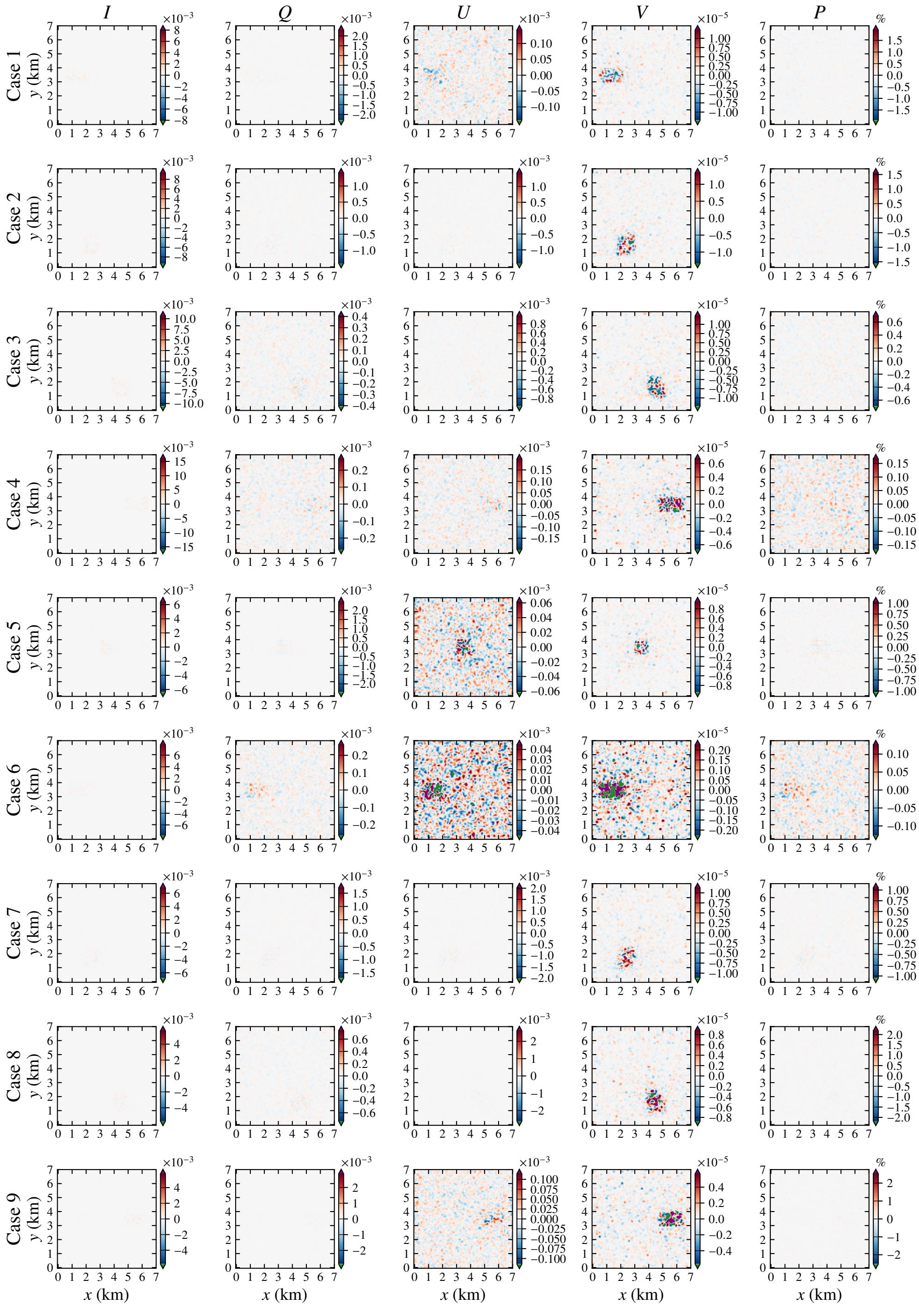

Figure S4. Similar to Fig. S2, except with MONKI in backward mode.

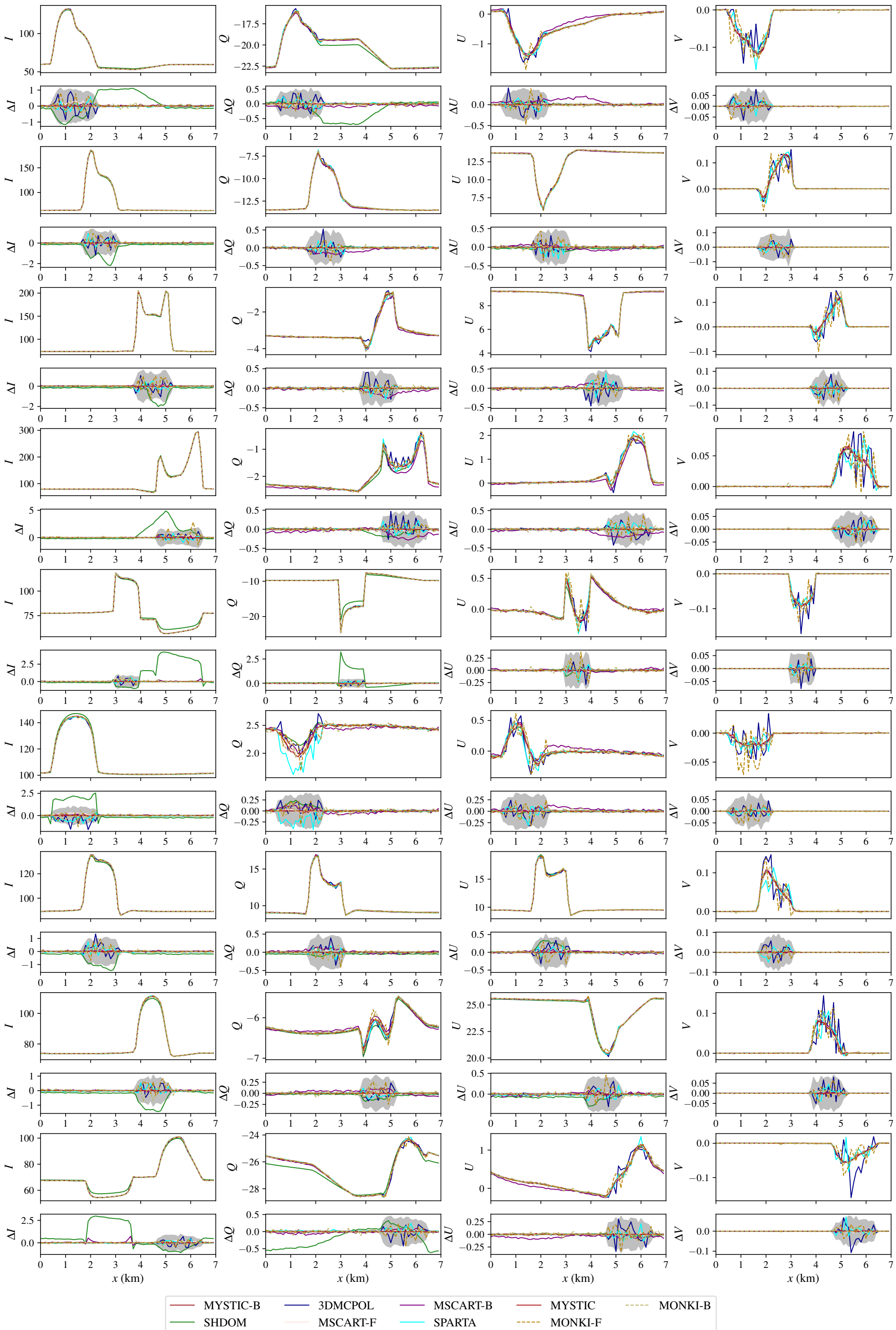

Figure S5. Similar to Fig. 6, except for the cases 1 to 9 (top to bottom row) with the geometries listed in Table S4.

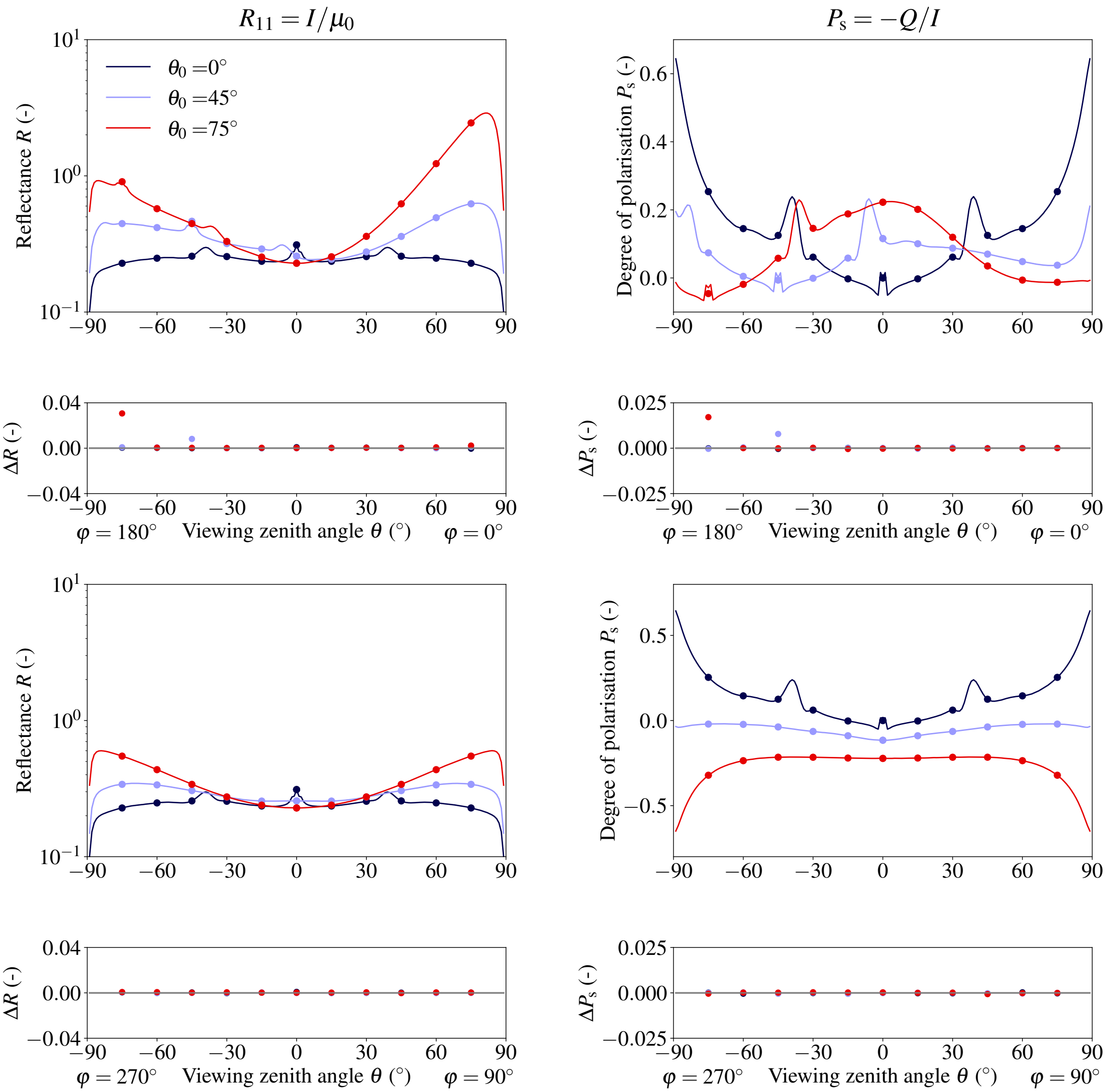

Figure S6. Comparison of the Earth model results of MONKI (solid lines) and DAK (dots) for the TOA reflectance R_{11} and the degree of polarisation P_s, at the azimuth directions ($\varphi = 180°$, $\varphi = 0°$) (top row), and ($\varphi = 270°$, $\varphi = 90°$) (bottom row). The solar azimuth angle $\varphi_0 = 0°$. The differences (MONKI−DAK) are also shown. For this comparison, MONKI used 10^9 photons per (θ_0, φ)-combination and 90 viewing zenith angles θ simultaneously. In DAK, 170 Gaussian quadrature points were used for both μ and μ_0, and 170 Fourier terms for the azimuth direction. This number of Gauss points in DAK explains the remaining differences between DAK and MONKI in the backscattering directions ($\theta_0 = 75°$, $\theta = 75°$, $\varphi = 180°$) and ($\theta_0 = 45°$, $\theta = 45°$, $\varphi = 180°$), where the sharp glory feature of the cloud droplets (at $\Theta \sim 180°$ in Fig. 9) is not fully resolved by DAK's Gaussian points.